



## Cavitation damage experiments for mercury spallation targets at the LANSCE – WNR in 2008

B.W. Riemer\*, M.W. Wendel, D.K. Felde

Spallation Neutron Source/ORNL<sup>1</sup>, P.O. Box 2008, Bldg. 8600, MS 6476, Oak Ridge, TN 37831, USA

### A B S T R A C T

Proton beam experiments investigating cavitation damage in short pulse mercury spallation targets were performed at LANSCE – WNR in July of 2008. They included two main areas for investigation: damage dependence on mercury velocity using geometry more prototypic to the SNS target than previously employed and damage dependence on incident proton beam flux intensity. The flow dependence experiment employed six test targets with mercury velocity in the channel ranging from 0 to more than 4 m/s. Each was hit with 100 WNR beam pulses with peak proton flux equivalent to that of SNS operating at 2.7 MW.

Damage dependence on incident proton beam flux intensity was also investigated with three intensity levels used on simple rectangular shaped targets without mercury flow. Intensity variation was imposed by focusing the beam differently while maintaining protons per pulse. This kept total energy deposited in each target constant. A fourth test target was hit with various beams: constant protons and varied spot size; constant spot size and varied protons. No damage will be assessed in this case. Instead, acoustic emissions associated with cavitation collapse were measured by laser Doppler vibrometer (LDV) from readings of exterior vessel motions as well as by mercury wetted acoustic transducers.

This paper will provide a description of the experiment and present available results. Damage assessment will require several months before surface analysis can be completed and was not available in time for IWSMT-9.

Published by Elsevier B.V.

### 1. Introduction

Mercury target experiments using the short pulse proton beam from the Los Alamos Neutron Science Center – Weapons Neutron Research (LANSCE – WNR) facility were conducted in July of 2008. These were the fifth in a sequence investigating cavitation damage in short-pulse liquid metal spallation targets [1,2]. Findings from previous experiments and off-line research motivated the scope covered in this campaign.

One issue for the SNS target concerns the narrow channels that supply cooling mercury to the proton beam entrance window (Fig. 1). These channels provide for well defined flow conditions at the window with mercury velocity reaching more than 3 m/s at the location of maximum heating from the proton beam. Prior in-beam experiments with stagnant mercury test targets and crudely mocked-up channels showed considerable cavitation damage on surfaces facing the channel even at locations outside the proton beam path [1]. These results suggested that the channels might be

the most damage vulnerable region of the SNS target and have stimulated consideration of a target design change that eliminates mercury channel flow. While alternative window cooling configurations can be addressed by changes to the SNS target design, the engineering and operational consequences are significant.

Conversely, other in-beam experiments that included mercury flow but dissimilar to SNS channel geometry demonstrated a reduction in damage with the introduction of flow [3]. With velocities achievable in the SNS target the channel damage might be sufficiently mitigated such that these regions are not the most likely to leak thus making a difficult design change unnecessary. Further experimental investigation of damage dependence on flow in channel geometry representative of the SNS target was needed.

Cavitation damage dependence on incident proton intensity (expressed as protons/pulse/area) remains another issue of concern. Off-line test results have generally indicated the long term (or high cycle) erosion rate is proportional to proton intensity raised to about the 4th power [1]. If true, the prospects for higher neutron source intensity (achieved via increasing proton power on target) could be challenging. Short term damage, or the so-called incubation phase of cavitation damage, progresses less aggressively. Previous in-beam experiment results have been inconsistent with respect to damage rate dependence on intensity. 2002

\* Corresponding author. Tel.: +1 865 574 6502.

E-mail address: [riemerbw@ornl.gov](mailto:riemerbw@ornl.gov) (B.W. Riemer).

<sup>1</sup> ORNL/SNS is managed by UT-Battelle, LLC, for the US Department of Energy under contract DE-AC05-00OR22725.

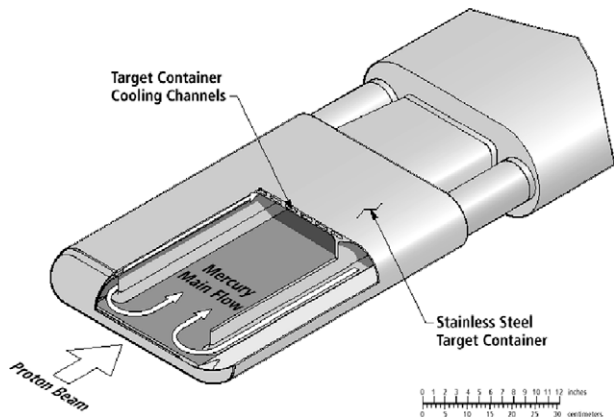


Fig. 1. Cutaway view of SNS mercury target vessel showing main mercury flow and the mercury cooling channels for cooling of the proton beam windows.

WNR results supported the stronger power law dependence (even though damage was clearly still in the incubation phase); results from the 2005 experiment did not [4]. More disturbing with the 2005 result was that: (1) damage did not monotonically increase with intensity and (2) a test condition common to 2002 and 2005 produced much less damage in 2005. A credible explanation has not been achieved. The 2005 experiment scope was therefore repeated in 2008.

Damage assessment of the embedded specimens was not completed by the time this paper was submitted. Following several months for radioactivity decay the targets are disassembled and specimens cleaned of removable contamination. Each specimen will be examined using both scanning electron and laser surface microscopes. Data for the fraction of eroded area and mean depth of erosion will be compiled for each test specimen and correlation to test conditions will be attempted by the end of 2009. Preliminary results from laser Doppler vibrometer (LDV) and acoustic detection of cavitation events are presented here along with a detailed description of the experiment.

## 2. Test objectives and methods

These mercury target experiments were performed at LANSCE – WNR with beam conditions generally similar to those used on previous occasions [1,2,4]. Proton energy was 800 MeV; typical pulses from the proton storage ring have an approximate pulse length of 0.3  $\mu$ s and a nominal full pulse contained ca.  $2.7 \times 10^{13}$  protons (4.3  $\mu$ C). Experiments were conducted in the so-called “Blue Room” that provides substantial space for a test apparatus and personnel access when the beam is off. The number of pulses on each target is limited to avoid excessive radiation in the room, and on this occasion pulses were limited to 100 per target.

Damage specimens were also prepared in similar fashion to previous tests except on this occasion all material was fully annealed type 316L stainless steel. The soft temper should provide for greater damage sensitivity to varied test conditions. Specimens were metallographically polished, indented with a  $5 \times 5$  array of microhardness indents as fiducial marks, and pre-test inspection was performed at each indent location using an SEM (Phillips XL30).

The test objectives were addressed with two types of mercury test targets described below.

Cavitation damage in short-pulse liquid metal spallation targets depends strongly on the incident beam conditions, therefore, measuring each beam pulse is critical to the interpretation of damage data. In previous tests the incident beam was measured using a flu-

orescing chromium-doped alumina (Chromia) plate that was monitored via mirrors by a shielded and radiation hard analog camera. An ORNL-developed image capture and analysis system combined with a LANSCE integrating current transformer provided quasi-real-time evaluation of beam size, shape, position and intensity (peak proton flux).

During this 2008 experiment campaign a parallel experiment was conducted to investigate advanced beam-profile diagnostic concepts for MW applications [5] that required hardware in the beamline which obstructed the usual view path of the Chromia plate. The beam diagnostic experimenters intended to provide an alternate target beam profiling system using a digital camera would outperform the older system. Unfortunately, the digital camera quickly failed despite considerable effort to shield the camera from radiation. Electromagnetic pulse effects may have contributed to the camera failure. A backup system using an analog camera and a frame-grabbing card from the old ORNL system was assembled in several hours that provided some real-time data for most of the pulses. Raw beam image data was saved that, in principle, could be analyzed later. Much of the pulse data for the first target test was lost, but the beam conditions appeared steady and data for pulses that were captured should be representative for that target, albeit with some added uncertainty.

A 0.125-mm thick copper foil was placed directly on the front of each target. Activation analyses of the foils will provide a measure of the integrated proton fluence profile on each target. This work is also incomplete at this time.

### 2.1. Damage dependence on mercury velocity in narrow channel

Four test targets were used to determine the effect of mercury velocity on cavitation damage, specifically for the near-prototypical narrow channel geometry. A test apparatus incorporating exchangeable target modules with a mercury pumping system was designed and named the Window Flow Vulnerability Test Loop (WFVTL). Mercury was circulated only through the target window channel region while the bulk mercury was stagnant. The design for this series of test targets is shown in Figs. 2 and 3 with comparison to SNS target channel dimensions shown in Fig. 4. The necessity for flat damage specimens (for metallographic polishing) led to some compromises in following the SNS channel shape. Photographs of targets are shown in Fig. 5.

A mercury pumping system was designed to provide channel velocities up to 7 m/s at the beam entrance location. The peak

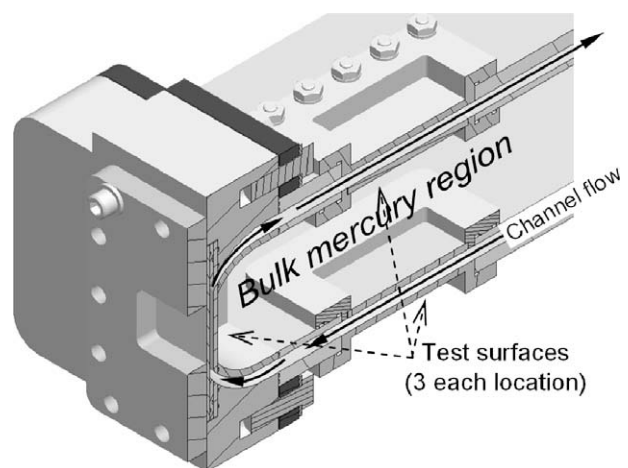
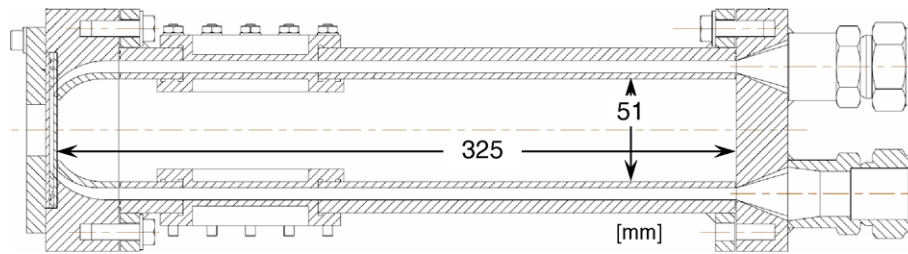
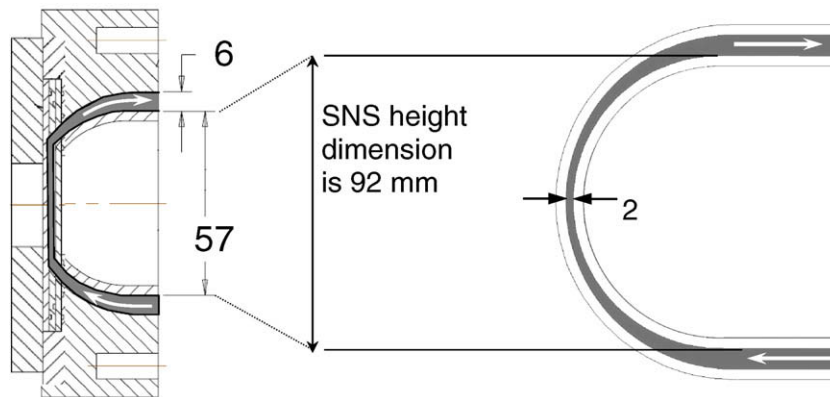


Fig. 2. A cross section view of the beam entrance end of the WFVTL target module. Mercury channel flow enters on the bottom; the channel narrows from 6 to 2 mm thickness at the beam window as it does in the SNS target.



**Fig. 3.** Elevation cross section view of a WFVTL target module. The flow channel width is 51 mm throughout. At the aft bulkhead this transitions to the supply and return connections to the pump system. The bulk mercury volume width is 143 mm. Modules were constructed with type 304L stainless steel while damage specimens were annealed type 316L stainless steel.



**Fig. 4.** To scale comparison view of window channel flow between the SNS (right) and WFVTL (left) targets. Channel thicknesses are the same. Arrows indicate flow direction.

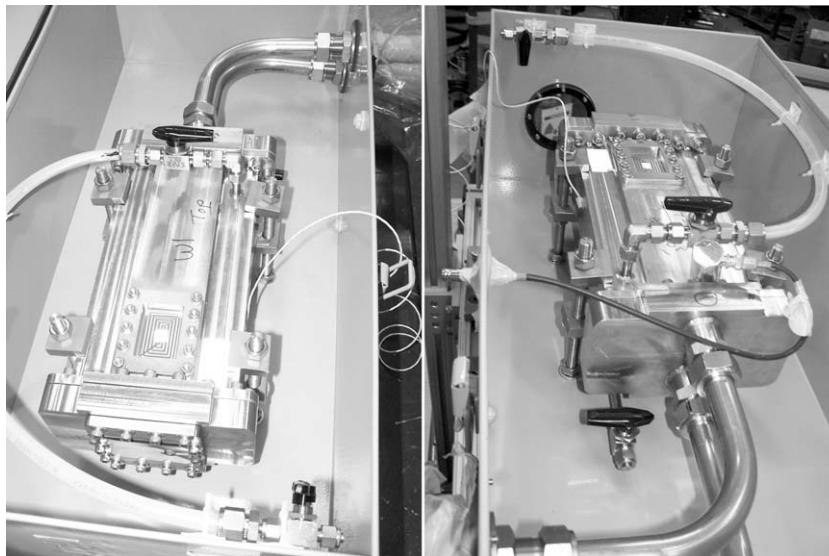


**Fig. 5.** WFVTL targets ready for irradiation inside their secondary containers. The plastic tube connects to the bulk mercury volume and includes some helium gas volume to allow for mercury expansion. The beam entrance window is covered with a copper foil to be later used for estimation of integrated proton fluence. An optical port in the secondary container box near the beam entrance end was used for LDV measurements.

SNS channel velocity is ca. 3.5 m/s at nominal system flow (24 l/s). A Kontro GTA CA3 stainless steel vertical pump was powered by a Siemens 3 Hp Explosion Proof Severe Duty 1750 rpm motor (460 V, 3 $\phi$ ). The pump should have provided up to 45 l/m of mercury at 2.1 m of total developed head to the test section. During testing prior to irradiation, the pump experienced two bearing failures and full performance was not achieved during the experiment. Only 4.4 m/s peak velocity at the window was possible at test time.

A storage tank at the bottom of the loop could hold the entire mercury inventory of 11 l. The system also included a heat exchanger with up to 800 W cooling provided by a Thermo Scientific NESLAB RTE-740 Digital One refrigerated bath.

The pump system was enclosed in a wheeled secondary container with a liquid-tight steel base and removable Lexan walls and top panels (Fig. 6). During irradiation these were tape-sealed except for some locations at the top. This allowed for some air in-

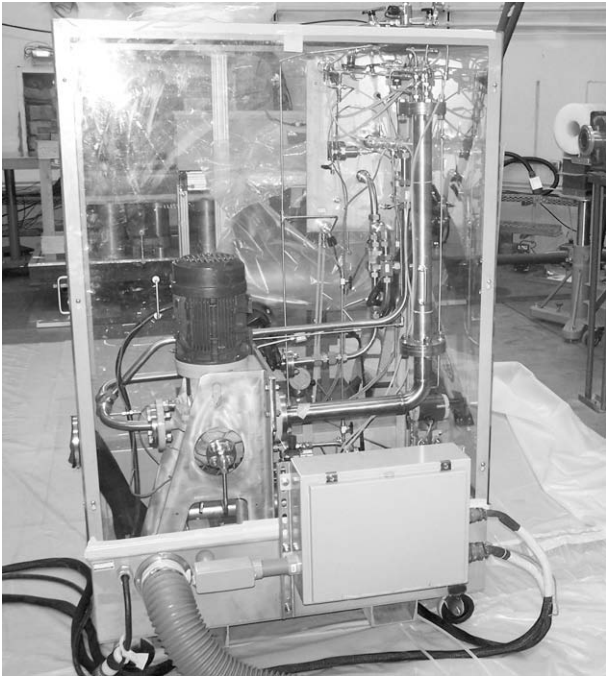


Fig. 6. WFVTL pump system prior to connection with a test target module.

flow as the container atmosphere was continuously vented through an AirFiltronix filtering system with mercury vapor and high efficiency particulate air (HEPA) filters during irradiations. The air ventilation duct can be seen in the lower left of the pump enclosure in Fig. 6 and power and control connections on the lower right. Flexible stainless braided hoses completed the mercury flow circuit to the target modules; these connected on the back side (as viewed from Fig. 6). During irradiation, lead blankets were positioned between the target and the pump loop to protect electrical components.

The pump system was controlled via an Allen Bradley 1756 ControlLogix system that provided programmable logic control

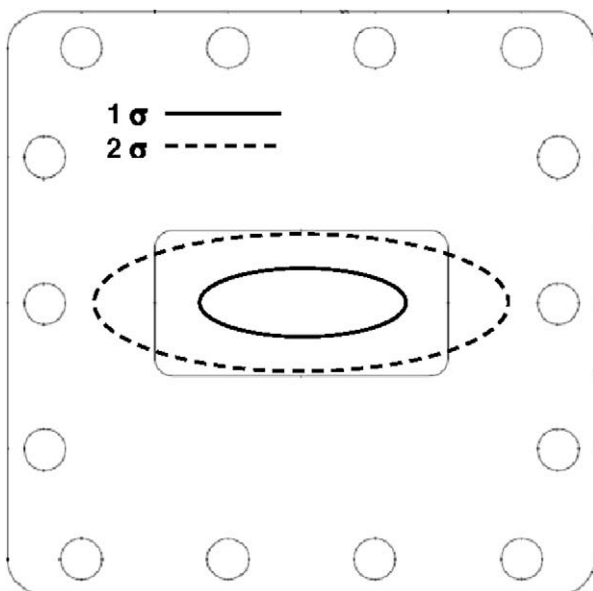


Fig. 7. Clamping plate for WFVTL beam entrance window. The rectangular window opening is 51 × 25 mm. Superposed are outlines for the desired 2D Gaussian beam profile at 1 and 2 sigma, with half width and height dimensions of 18 and 6 mm.

and measurement of system operating parameters. Levels in the pump reservoir and the storage tank were measured with Foxboro Model IDP10 differential pressure transmitters. Loop pressure was measured at several locations using Viatran pressure transmitters. Mercury fluid temperatures were measured using platinum resistance temperature detectors. Pressure relief valves were located at several locations around the loop to protect loop components from overpressure, including the gas supply line that was set to relieve at 690 kPa. The PLC control cabinet was connected to the system and the pump motor starter/VFD controller via ~50 m of cable to allow positioning of the cabinet outside of the beam room.

Temperature and pressure were monitored by the control system which also provided for automatic shutdown of the pump and draining of the mercury inventory to the storage tank if safety limits were exceeded. Interlocks on solenoid valves and pump operation ensured proper sequencing of valves during fill and drain operations as well as settings for pump operation. Check valves on the gas lines prevented back-flow of mercury to the gas supply system. Actions of interlocks and check valves were verified during shakedown testing of the system.

A mercury vapor filter was installed on the gas vent line at the top of the loop to prevent release of mercury vapor from the loop. Periodic monitoring of the output from the filter for mercury vapor verified adequate filtration.

Each WFVTL target module incorporated damage test surfaces at three locations: at the beam entrance window, the bottom channel and at the top channel. At each location two surfaces faced the channel mercury and one faced the bulk mercury. The inner specimen at the beam entrance window was slotted for the channel flow. All damage test specimens were made from type 316L stainless steel (the SNS target vessel material) in the fully annealed condition.

The clamping plate for the beam window damage specimens featured a 25 × 51 mm opening (Fig. 7) through which the beam passed. Based on prior WNR experience a typical beam pulse was presumed with  $2.7 \times 10^{13}$  protons per pulse. The desired beam profile of  $\sigma_x = 18$  and  $\sigma_y = 6$  mm (half width and height) would have provided a peak proton intensity equivalent to that for 2.7 MW SNS operation with its design basis beam profile.

Actual beam conditions were recorded on a shot by shot basis from the aforementioned backup imaging system. A photograph of the Chromia screen (consisting of two plates) is shown in

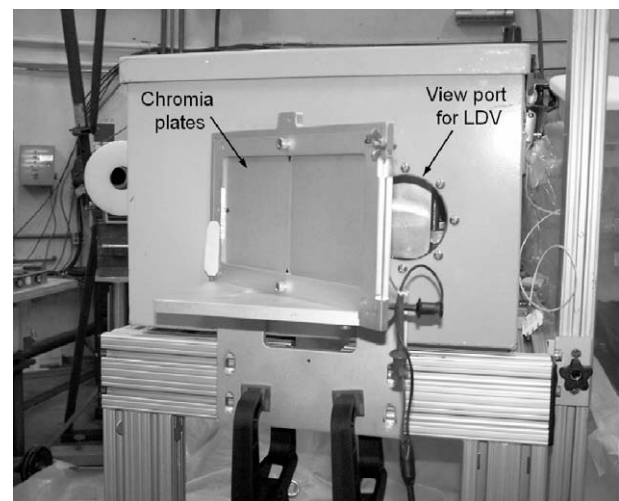


Fig. 8. Chromia beam imaging plates in front of a WFVTL target secondary container. The plate fixture was aligned to the target and beam axes with the help of a double ended laser simulating the beam and an alignment fixture that transferred the target axis to the plate.

**Table 1**  
Target test conditions.

Target name	Peak channel velocity (m/s)	Average protons /pulse $\times 10^{12}$	Average $\sigma_x$ (mm) <sup>a</sup>	Average $\sigma_y$ (mm) <sup>a</sup>	Average max. intensity (p/mm <sup>2</sup> $\times 10^{10}$ ) <sup>b</sup>	Intensity standard deviation (% of ave.)	Comment
W4-7	0–4.4	19.9 <sup>c</sup>	16.4	7.7	2.51	29.0	LDV testing only; range of channel velocities employed
W3	3	27.0	17.3	8.0	3.10	4.4	
W1	1–2 <sup>e</sup>	27.0	18.3	7.9	2.95	3.9	
W2	4.4	26.8	17.4	8.0	3.08	3.4	Max. possible vel.
W0	0	26.9	17.5	7.3	3.37	3.5	
WW	0	25.9	18.5	8.4	2.66	3.0	Water in channel
RLDV	n/a	0.13–27	15–34	4.6–10	0.05–5.6		LDV and PCD testing; range of beam parameters employed
RH	n/a	26.5	15.4	5.2	5.25	3.3	
RM	n/a	26.6	20.2	6.1	3.43	2.6	
RL	n/a	26.3	32.4	9.4	1.36	4.2	
RTX	n/a	26.5	21.2	6.7	7.15	2.4	
RLP	n/a	45.4 <sup>d</sup>	20.4	6.1	6.0 <sup>d</sup>	5.7	833 $\mu$ s pulse

<sup>a</sup> Half widths and heights.

<sup>b</sup> Maximum intensity based on Gaussian fit dimensions averaged over credible pulse data.

<sup>c</sup> Proton beam diagnostics were marginally functional during W4-7 irradiation.

<sup>d</sup> RLP proton count data obtained for only six pulses; profile data obtained for most pulses.

<sup>e</sup> W1 channel velocity uncertain because of failing sensor.

Fig. 8. As shown, the two square plates meet on the beam axis. The uneven scintillation between plates caused a difficulty with the acquired images. Later a spare plate was split and installed in the frame so that a joint was not on the beam axis.

In order to match the SNS target local static pressure, 69 kPa (10 psi) overpressure was applied to each WFVTL target mercury channel.

Target test conditions are shown in Table 1 in the order of testing. Targets used to investigate velocity effects were: W0, W1, W2 and W3. The first six tests were WFVTL related target tests. The goal was keep the incident beam profile conditions constant for all WFVTL targets based on the schematic shown in Fig. 7. Included in Table 1 are the beam measurements obtained from the online beam diagnostic system. A Gaussian profile fit was made to horizontal and vertical slices of beam images that were obtained from the Chromia plates. Analyses have since shown that the Gaussian assumption does not hold well for many conditions, but the Table 1 values are accurate enough for condition comparison. Analysis of the beam data continues; a more accurate description is needed for correlation to damage statistics.

Disconnection and reconnection of the flexible steel reinforced hoses between target module and pump system were challenging



**Fig. 9.** WFVTL target secondary container (left) with mercury hoses for connection to the pump loop inside the spill/vapor tub (right). The pump loop is just out of view on the right. A ventilator duct connects to the tub end opposite of where hose connections were broken and remade.

aspects of the experiment because of the personnel radiation and mercury exposure safety issues. The procedure practiced at ORNL proved inadequate for mercury drip and vapor control when tested in full configuration at the WNR and required improvement prior to irradiation. A plastic tub with a hinged lid was used containing the hose connectors. The tub was ventilated with the HEPA/mercury filtration system. Fig. 9 shows the tub and hoses in the near final configuration. Shield blankets were later draped over the target and hung on stands to further protect the worker doing the hose connection procedures. This operation took about five minutes of time with the work in close proximity to the target and pump system. The worker wore a full contamination suit, respirator with HEPA and mercury filters and multiple glove layers.

## 2.2. Cavitation damage potential estimate from LDV measurement as function of mercury velocity

The very first WFVTL target irradiated was dedicated to obtaining laser Doppler vibrometer (LDV) data for a range of channel flow velocities. Surface damage will (erosion) not be measured for target W4-7. The use of the LDV data will be discussed below but by doing this target first the final configuration for the LDV setup could be established for the remaining WFVTL targets. Two locations for monitoring surface motion were provided, but ultimately the most sensitive position was on the beam entrance window of the target about 20 mm horizontally offset from the beam axis. The laser was incident at this location obliquely through a viewport in each secondary container (Figs. 8 and 9).

## 2.3. Confirmation of water window coolant being non-damaging

If the particular damage vulnerability of the channel is confirmed from this experiment, one possible solution is redesign of the SNS target using water to cool the beam windows. The WFVTL target “WW” used stagnant water in the cooling channel instead of mercury to confirm that using water would reduce the cavitation damage in the narrow channel without making the bulk-side damage any worse.

## 2.4. Damage dependence on incident proton beam intensity

Damage dependence on incident proton beam intensity was investigated using three stagnant mercury-filled rectangular test

targets of a type used in previous experiments [1,2,4]. A photograph of a rectangular target prior to irradiation is shown in Fig. 10. The method here was to hold protons per pulse constant for each test conditions and vary intensity (peak protons per unit area) by changing the beam spot size as shown in Fig. 11. The largest spot size just fit inside the target at  $2\sigma$  which kept total deposited beam energy nearly constant for all three conditions. Three targets (RH, RM and RL for high, medium and low intensity) were used with the beam parameters shown in Table 1.

### 2.5. Cavitation damage potential estimate from LDV measurement as function of proton intensity; passive cavitation detection

The rectangular target series actually began with target “RLDV” which was dedicated to obtaining acoustic emission data associ-

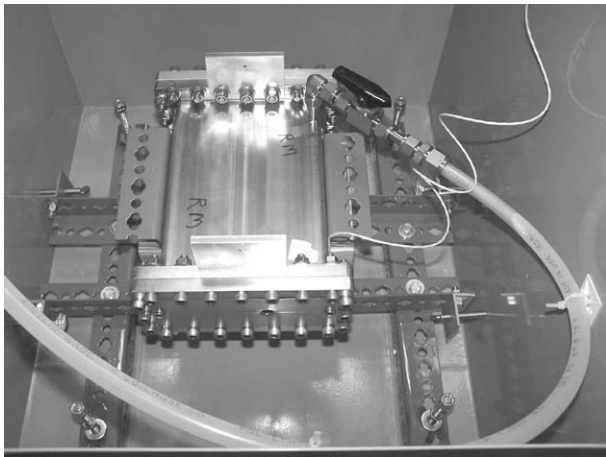


**Fig. 10.** Rectangular target used for beam intensity and long pulse investigations. The beam entrance is covered with a copper foil that will be analyzed for proton fluence profile. A 1 cm hole off of target axis provided line of sight viewing to the target entrance window for LDV measurements. Mercury dimensions were  $41 \times 143 \times 229$  mm ( $H \times W \times D$ ).

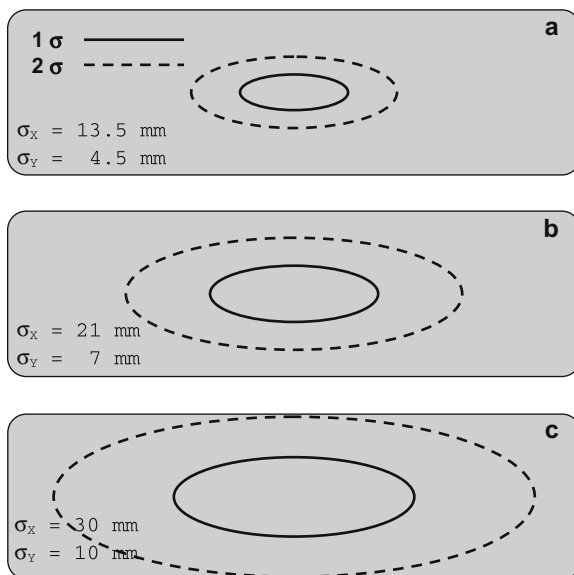


**Fig. 11.** Beam profile goals for rectangular target high, medium and low intensity conditions (a–c, respectively). One and two sigma Gaussian profiles are drawn to scale on top of the target mercury outline. Assuming  $2.7 \times 10^{13}$  protons per pulse the peak intensity for a–c would correspond to SNS operating at 4.8, 2.0 and 1.0 MW with its nominal beam profile.

ated with cavitation bubble collapse. A wide range of incident beam conditions with varied protons per pulse and spot size were explored. Damage on the specimen plates will not be measured. The LDV tracked a spot on the beam window approximately 20 mm horizontally offset from the center.

RLDV also uniquely incorporated two acoustic immersion transducers inside the mercury volume mounted via feed-throughs in the target rear window and used for passive cavitation detection (PCD). Both were made by Olympus – Panametrics; one was a 2.25 MHz, 25.4 mm element diameter, 200 mm spherically focused transducer (Model V304); the other was a 1 MHz, 19.05 mm element diameter, unfocused transducer (Model V314). Fig. 12 shows the PCDs mounted in the rear window prior to installation in the target. Fig. 13 shows RLDV just prior to irradiation.

A low frequency sensor (Physical Acoustics model R.45, 5–30 kHz) for external monitoring of acoustic emissions is shown on the top of target RLDV. Unfortunately, its required preamplifier failed possibly caused by electromagnetic pulse effects of the beam.

### 2.6. Textured wall surface for enhanced gas wall coverage

SNS R&D activities for damage mitigation include investigations of protective gas layers between the target mercury and vessel wall

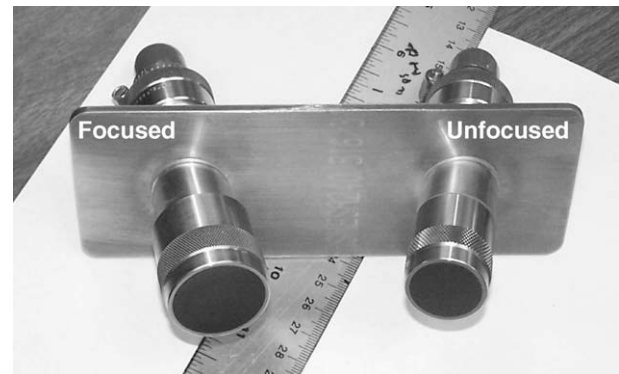


**Fig. 12.** Passive cavitation detection transducers mounted in the RLDV rear window. The transducers were angled to intersect at the front window and beam axis.

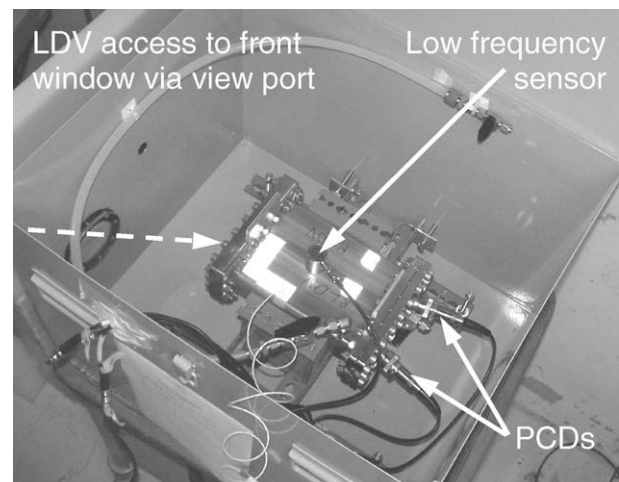


**Fig. 13.** RLDV Target prior to irradiation. The position of the passive cavitation detection (PCDs) transducers is noted along with the externally mounted low frequency sensor and path for LDV measurement of the target front window.

[6–8]. One challenge is to maximize the gas wall area coverage in flowing mercury systems. Two-phase flow experiments in the ORNL Target Test Facility have demonstrated enhanced coverage when the vessel wall is textured with small machined grooves or pits with steep sidewalls (ca.  $60^\circ$  from the surface) and a spacing of about 0.5 mm. Damage resistance of a gas layer enhanced by texturing was investigated using target RTX with stagnant bulk region and a textured front window, again subjected to 100 medium-intensity short beam pulses. A flowing target gas wall experiment was beyond capabilities for this test campaign.

The front window of RTX was machined with conical pits and gas was injected through a port below the beam axis. An initial gas condition at the wall was reestablished after each beam pulse by remote operation of a solenoid controlled gas valve. Excess gas was vented from the target through a mercury vapor filter.

Offline testing with an acrylic version of the textured window showed that gas injected at the base of the window would stay on the wall in the area of peak beam intensity. A photograph from that test is shown in Fig. 14; the light area indicates gas stuck to the wall. A micrograph of the textured steel window is shown in Fig. 15. Damage assessment may present added difficulty compared to the usual flat and highly polished surfaces.

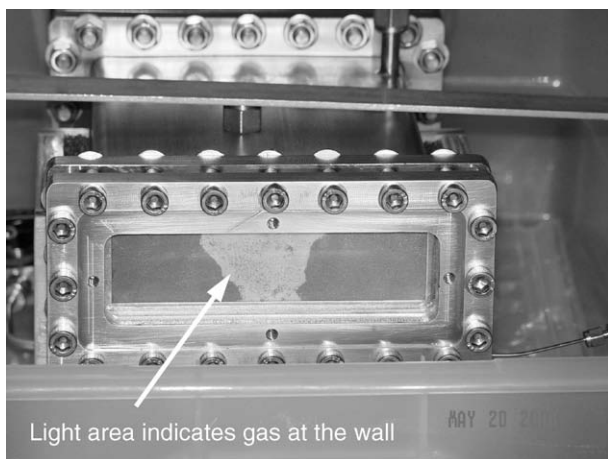


**Fig. 14.** Acrylic window version of RTX target filled with mercury undergoing test. Gas is puffed from a port directly under the beam axis; the texturing holds gas at the wall as indicated by the light colored area.

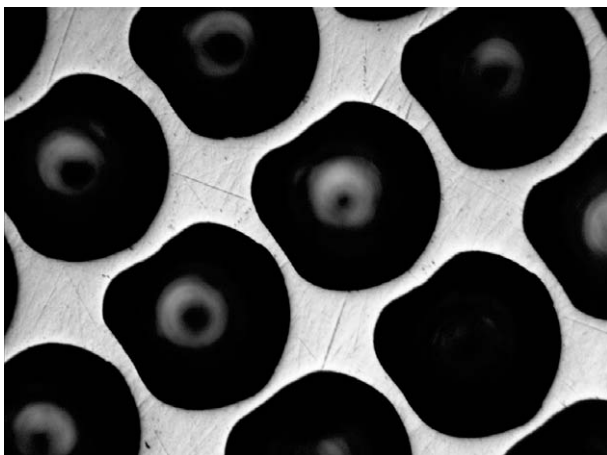


**Fig. 15.** Microscope image of steel window with pit texturing. The surface was polished after texture machining to clean up burrs and provide some flat surface for damage assessment. The spacing between pits is ca. 0.5 mm.

## 2.7. Damage from long beam pulses

The SNS beam pulse lasts less than  $1 \mu\text{s}$ ; this is considered a short beam pulse. It is this rapid deposition of energy into the mercury that leads to cavitation phenomenon in the target. A second target station for SNS is proposed that will use a long pulse beam, i.e., pulse length of about 1 ms ( $10^{-3}$  s). While the propensity for cavitation should be much lower for long beam pulses, it is not certain that a higher power, lower frequency long pulse mercury target would be immune to cavitation damage. Given the interest in this issue at SNS and elsewhere and the opportunity during this WNR experiment campaign, the objective to assess damage for 100 long pulses from the LANSCE accelerator was added to the test scope.

Target RLP was irradiated with 100 pulses of 800 MeV protons with a pulse length close to 1 ms and the same beam profile that was used for target RM. The intention was to have pulses with the same number of protons as with short pulse tests. There were difficulties in measurement of the long pulses but it turned out that significantly more protons per pulse were applied.

## 2.8. Fluorescence of sprayed chromium-doped alumina on steel

This test objective was born out of a desire to have beam-profile diagnostic directly on the SNS target face [5]. One option under consideration is direct application of a fluorescing material to the front exterior of the target module. The front of the SNS target could be viewed from a mirrored portal in the proton beam window assembly that separates the SNS core vessel environment from the accelerator beam line. Chromia plate is commonly used as an accelerator beam-profile diagnostic as it was here. For this experiment objective, steel coupons were sprayed with various mixtures of Chromia by two development processes. Five coupons were evaluated for fluorescing intensity and uniformity.

Tennessee Metalizing provided a set of flame sprayed samples approximately  $25 \times 75$  mm in area with three different chromium oxide doped alumina compositions – 0.5%, 1% and 5% of chromium oxide. Each sample coating was approximately 0.25 mm thick on top of 1 mm thick steel plate. Two samples provided by Praxair used their “D-gun” process. These were approximately

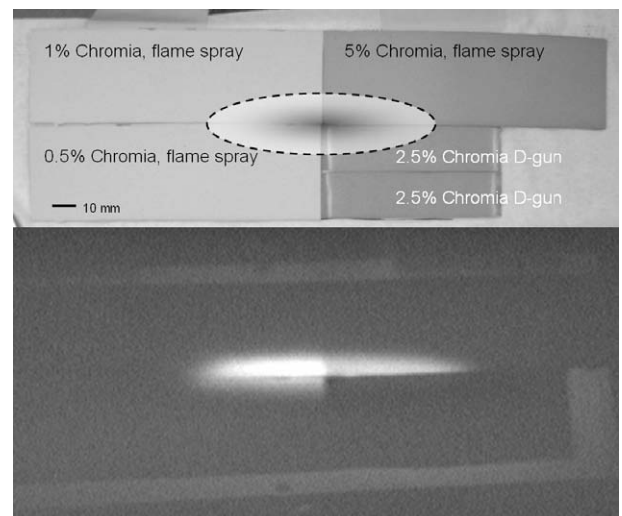


**Fig. 16.** Top: Five steel test coupons coated with chromium-doped alumina assembled for simultaneous proton irradiation. The two smaller coupons on the lower right were of identical composition. Bottom: Example image of fluorescence from a proton pulse. The brightest was the 1% flame sprayed coupon. Neither D-gun sample fluoresced at all.

13 × 50 mm, both with 2.5% chromium oxide; one was 0.25 mm thick and the other 0.46 mm. The five coupons were arranged for simultaneous testing as shown in the top of Fig. 16 and later mounted in the beam line as illustrated.

### 3. LDV setup, data collection and analysis

LDV data has previously been used to obtain a so-called damage potential parameter which was successfully correlated with measured damage [3]. LDV data was obtained from all 2008 target tests and correlation to measured damage on the specimen plates will be attempted.

These experiments utilized a Polytec laser vibrometer model OFV-5000 controller, OFV-505 sensor head with OFV-SLR lens, and Vibsoft software for data acquisition and analysis. The sensor head was kept 15 m away from the target behind shield walls by using a long range lens and was relatively well protected from irradiation. The LDV control unit and computer were located outside the Blue Room. The laser viewed a spot on each target front beam window via two mirrors, and there was no direct line of sight from the target to the sensor head. A special reflective tape was applied to the exterior of the target to enhance reflection; the laser hit the target window through the view port on each target's secondary container at an angle of approximately 30° off perpendicular to the surface normal. This setup was mocked up and demonstrated at ORNL before arriving at LANSC. One unknown prior to irradiation was the optimal spot on the targets to maximize sensitivity to surface motion without saturating the instrument. The vibrometer configuration had a maximum velocity range of ±10 m/s. If the front beam window velocity amplitude exceeded this value (saturated signal) then an alternative location on the top of the targets was also available.

The full bandwidth (2.0 MHz) of velocity data was stored for every beam pulse by the data acquisition software, but processing on the fly was also performed to provide a preliminary estimate of the so-called damage potential parameter (CDP), a measure of cavitation collapse intensity and predictive indicator for damage [3]. Macros for the analysis software were written to automate this task. Each velocity response was band pass filtered (15–300 kHz); velocity values were then squared and summed to provide the time integrated parameter result. The saved unfiltered raw data allows for further data analysis, for example, with different pass frequencies or with wavelet analysis techniques. Here CDP is equivalent to  $E_H$  in [3].

### 4. Post target irradiation work

Targets were drained of activated mercury about six weeks after irradiation; targets, mercury and all equipment were shipped back to ORNL in September 2008. Disassembly of targets to extract damage test specimens and their decontamination is planned to begin in February 2009. Altogether there are 40 damage specimens with 60 surfaces to clean and analyze. Specimens must be free of removable contamination and pass a test for the presence of mercury vapor.

Surface examination will employ a scanning electron microscope and a laser profile microscope. SEM images will be taken at the fiducial locations established prior to where images were taken prior to irradiation, some 50 images per surface or 3000 images altogether. An image comparison process will provide a measure of fraction of eroded area for each image. The laser microscope will measure damage pit morphology and provide estimation of mean depth of erosion. Compilation of the damage at the worst locations for each test condition will be made and correlation to conditions will be attempted.

Results regarding damage vulnerability of the window channel will be used along with post irradiation examination of the first SNS target to direct any redesign of the SNS target.

## 5. Results

As mentioned above, damage analysis of the test surfaces has not been completed at this time. Initial results from the laser vibrometer and passive cavitation detectors will be presented below, preceded by some general observations from the experiment.

The difficulties with the beam diagnostic system described earlier made precise determination of pulse by pulse conditions more ambiguous than desired for some test conditions, in particular with target W4-7 and to some extent for W3 and RLP. Improved measurements are possible from raw beam profile image and current data and work is in progress to make the most of what is available. Analyses completed so far of beam profile images produced the Gaussian fit parameters but it is clear that the actual profiles are not Gaussian. The fits are convenient for general comparison but do not provide the best prediction of peak proton intensity. After noise filtering of the raw image data is complete, better peak intensity values will be available.

The WFVTL pump was not able to provide the design flow performance due to two bearing failures that occurred late in testing prior to shipment to LANSC. Even though this pump is sold for industrial mercury pumping applications this choice for research use was a mistake. The frequent on/off cycling and repeated draining and filling encountered during research is apparently quite different from and incompatible with typical industrial usage.

Some instrumentation of the loop system failed with accumulated radiation exposure. The differential pressure transmitters on the venturi flow meter, the pump reservoir level and the storage tank level failed. These were all the same type instrument: Foxboro Model IDP10 differential pressure transmitters. The pressure transmitters were all Viatran models and did not appear to have any problems. There were no problems with any resistance temperature detectors, possibly because electronics for these sensors were located far from radiation sources. All other loop system electronics were in an instrument cabinet located far from the radiation sources and operated without any problems.

### 5.1. WFVTL

LDV data from the WFVTL targets has been and continues to be analyzed. Fig. 17 shows two examples of velocity data obtained from targets W0 and W1. The total time of data captured was 0.2 s but here only 12 ms is displayed. The effects of the CDP processing steps can be seen in Fig. 18 using the W0 example data. Additional processing conditions have been imposed beyond those described in Section 3. Velocity data beyond the first 4 ms captured were not used in calculation of CDP because by this time a maximum had typically been achieved with time integration. The first 10 μs of data after the pulse were also excluded in CDP because the wall's prompt response contributes significantly to the CDP but is not associated with cavitation bubble collapse. In the case of target WW this excluded period extends to 15 μs after the pulse. The CDP values obtained for all the beam pulses on each target were averaged together and the results are summarized in Table 2. Results from W4-7 are shown as a function of channel velocity.

The quality of the velocity data varied from target to target. Signal dropouts occurred with some targets and were prevalent throughout target W1 irradiations. The dropouts are manifested as sharp spikes in the raw data as seen in the W1 example in Fig. 17. The cause of the dropouts is so far unknown although consultation with Polytec continues regarding the issue. The frequency

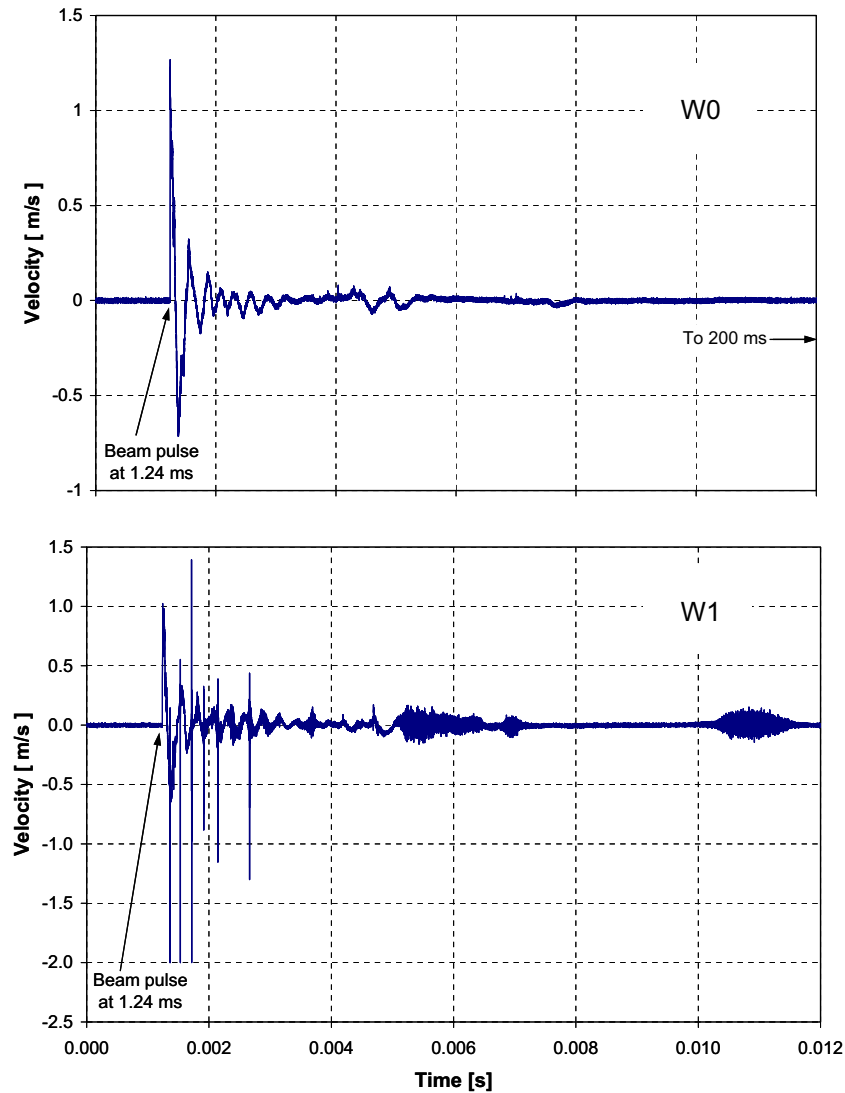


Fig. 17. Example raw velocity data from targets W0 and W1. W1 data suffered from signal dropout as evidenced by the multiple sharp spikes.

content of the spikes was within the desired bandwidth and falsely contributed to accumulated CDP. Therefore the data summarized in Table 2 represents average results from a subset of all pulses for a given target chosen by manual scrutiny of the raw velocity data. There remains notable scatter in the estimated CDP as shown by the standard deviations in Table 2. No useful CDP result is yet available for W1; an attempt will be made to repair the dropout data.

The average protons per pulse and peak intensities corresponding to Table 2 CDP results are included in Table 1. Except for W4–7 the beam charge and intensity data were very steady for WFVTL targets. Unfortunately beam diagnostic problems during W4–7 irradiation leave a less clear picture of how the beam was applied. What data there is for W4–7 indicates the average protons were  $20 \times 10^{12}$  with considerable scatter. Nevertheless CDP results are shown broken out for three channel velocities from W4–7. There is some decrease with the introduction of flow but little difference between 3.0 and 4.4 m/s. Similarly with targets W0, W2 and W3, a decrease in CDP is seen with the introduction of flow but little difference between 3.0 and 4.4 m/s.

The results for the target with water in the channel (WW) showed a CDP somewhat lower than W0 but still larger than any flowing mercury or W4–7 condition.

## 5.2. Rectangular target results – beam intensity

Cavitation damage potential estimates for targets RH, RM, and RL are summarized in Table 3 and show an increase in CDP with increasing peak proton intensity (refer to Table 1 for intensities). Protons per pulse were consistently applied between these three tests. The standard deviation in peak intensity varied no more than 4.2% for each condition.

The low intensity target (RL) showed an unusual but consistent feature in the accumulation of CDP. Fig. 19 shows CDP accumulation from example pulses from RH, RM and RL. RL has a step-like increase between 3 and 4 ms that is not the result of a signal dropout. Its origin is not understood.

## 5.3. RLDV target

CDP results from the RLDV target with high and medium beam profiles applied are consistent with those from RH and RM. The unusual step increase seen in RL is also seen with RLDV when the low intensity profile was applied. However the magnitude of the step is much greater – so much so that CDP from the low profile is higher than that from a high intensity pulse. The average result is about  $1.0 \text{ mm}^2/\text{s}$ .

A wide range of beam charges was explored from about 0.02 to 4.3  $\mu\text{C}$  ( $0.13$  to  $27 \times 10^{12}$  protons). With beam spot size adjusted to

the medium intensity profile CDP became evident at a charge of 0.04  $\mu\text{C}$ . CDP increased consistently with increasing charge.

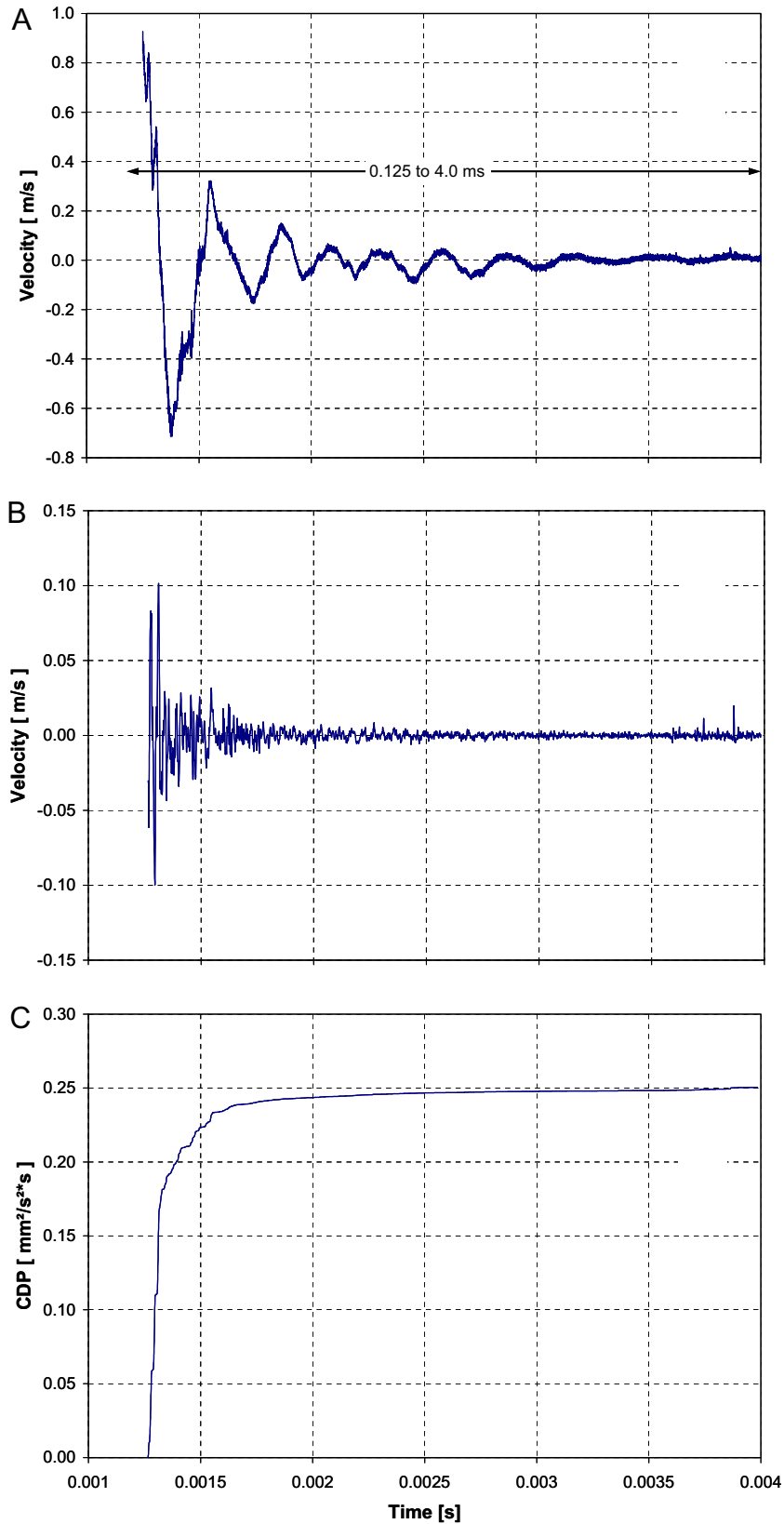


**Fig. 18.** The effect of the steps taken for obtaining CDP data are shown on the W0 raw data example from Fig. 17. (A) The range of data processed extends only to 4 ms and skips the first 10  $\mu\text{s}$  after the beam pulse. (B) A bandpass filter passes only velocity data in between 15 and 300 kHz. (C) Time integrating the square of the filtered velocity data produces the CDP parameter.

**Table 2**

Cavitation damage potential from WFVTL targets.

Target	Peak channel velocity (m/s)	CDP (mm <sup>2</sup> /s)	Std. deviation
W4-7	0.0	0.132	0.052
W4-7	3.0	0.095	0.014
W4-7	4.4	0.101	0.015
W3	3.0	0.124	0.012
W1	1.0	<sup>a</sup>	
W2	4.4	0.128	0.035
W0	0.0	0.365	0.113
WW	0.0	0.312	0.053

<sup>a</sup> Data quality unusable for W1.**Table 3**

Cavitation damage potential from rectangular targets and predicted normalized damage area.

Target	CDP (mm <sup>2</sup> /s)	Std. deviation	$A_c/A_0$
RH	0.160	0.090	1.48
RM	0.083	0.012	1.00
RL	0.062	0.063	0.84
RLP	<0.0003		<0.03

The use of embedded acoustic transducers to capture acoustic emissions from cavitation was successful. The focused PCD transducers could clearly detect cavitation activity beginning at a charge of 0.2  $\mu\text{C}$  (Fig. 20); at 0.08  $\mu\text{C}$  indications are debatably distinguishable from noise. At 0.4  $\mu\text{C}$  the unfocused transducer could also detect cavitation emissions. No clear difference in cavitation signals could be inferred when changing the beam profile with charge at full magnitude.

The sensitivity of transducers decayed significantly with increasing pulses, but they still functioned. This was occasionally tested by sending an active pulse signal from one transducer that would reflect inside the target and be received by the other transducer. Radiation damage was suspected at first. Sensitivity fell to less than 2% of pre-irradiation level by the end of the test. However, sensitivity recovered after irradiation and after about 12 h it had nearly returned to its original level. A possible explanation is that bubbles gradually formed on the transducer surfaces during irradiation that impeded acoustic coupling with the mercury. Over

time these might have dissolved or floated away, thus restoring sensitivity. A separate paper is under preparation by collaborators at Boston University to describe the use of PCDs in this experiment and provide detailed results.

#### 5.4. Textured surface gas wall target results

CDP results for the textured surface target show very large variation ranging from 0.03 to 0.23 mm<sup>2</sup>/s even though beam was steadily applied. Gas puffing may not have been performed properly during the test. It was determined after testing that a protective cap on the gas vent line was still installed although loose. It is unclear how significantly this inhibited gas puffing.

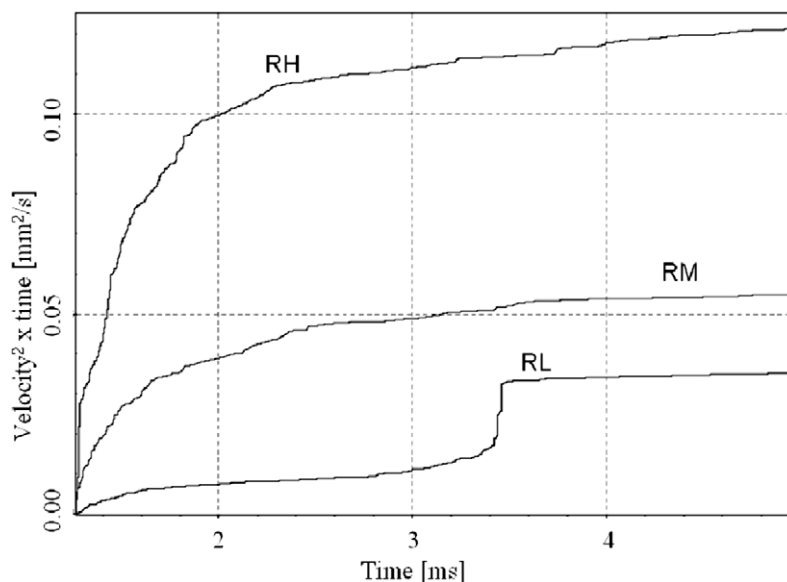
#### 5.5. Long pulse target results

CDP for target RLP is also included in Table 3. The upper bound value is more than two orders of magnitude lower than for RM and it is the result of noise remaining in the band-passed velocity data. Based on this LDV data there is no indication of cavitation. While beam profile data was adequately captured by the beam diagnostic system for RLP (standard deviation of profile dimensions is less than 4.5% of average), the protons per pulse were not. Only one pulse charge was completely captured out of 100 and it was considerably larger than the typical short pulses. It had  $44.4 \times 10^{12}$  protons (7.1  $\mu\text{C}$ ) and a measured pulse length of 833  $\mu\text{s}$ . Five other pulses were mostly captured with some of their tails missed. By integrating over a 400  $\mu\text{s}$  portion of each partly captured proton data trace and extrapolating to 833  $\mu\text{s}$  a full charge value was estimated for those pulses. The average protons and intensity reported in Table 1 for RLP are based on these six pulses.

Activation analysis of the copper foil will provide a measure of total protons on RLP for all 100 pulses from which these limited per pulse estimates can be confirmed.

#### 5.6. Fluorescence of sprayed chromium-doped alumina

Only four pulses were needed to demonstrate that the flame spray Chromia successfully fluoresced while the D-gun spray application did not. An image from one pulse is shown in the lower part of Fig. 16. The 1% flame sprayed coupon gave the brightest illumina-

**Fig. 19.** Rectangular target cavitation damage potential vs. time from example pulses from each intensity conditions.

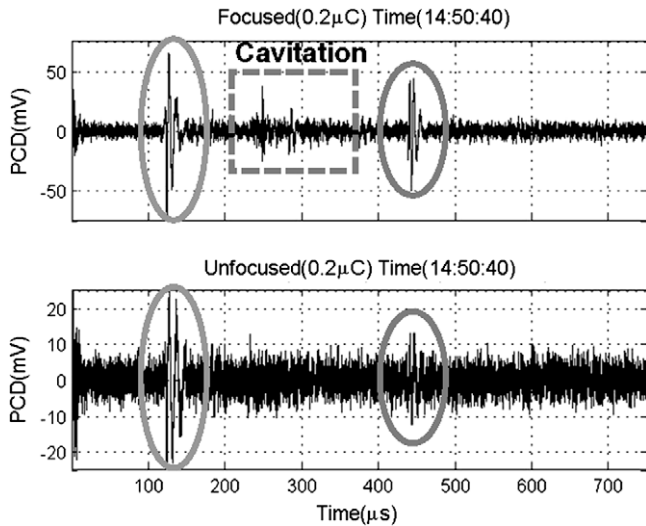


**Fig. 20.** Signal from acoustic transducers embedded in RLDV target responding to a beam pulse charge of  $0.2 \mu\text{C}$ . The circled features are reflected pressure waves emanating from the front beam window. The boxed features in the focused transducer trace indicate cavitation activity. From Nicholas Manzi, Boston University, with permission.

nation and was comparable to the standard Chromia plates. Subsequent analysis has shown that the flame sprayed material retained a high percentage of alpha phase alumina while the “D-gun” material had very little alpha phase. This is believed to be the main reason for the difference in brightness.

## 6. Discussion

The change in CDP with the introduction of flow suggests that damage should be less with flow but also that more damage reduction cannot be expected with increasing velocity. The change in CDP from 3.0 to 4.4 m/s flow is insignificant. The change from stagnant to flow is larger comparing W0 to W2 and W3, vs. W4–7 with no flow to with flow. This difference is puzzling; it may be more than can be explained by uncertainty in imposed beam with W4–7. It is to be noted target W0 had its flow channel capped at the back end and was not connected to the pumping loop. By contrast W4–7 was always connected to the loop even when mercury was not being circulated.

The CDP result for WW was higher than expected. WW was similarly not connected to the loop and had its flow channels capped at the back of the target. Perhaps that difference is more significant than is understood. The relatively high CDP for WW is a concern if it is to be believed, inferring that water might not be a cure to the special damage vulnerability of the channel. Damage assessment, as with all targets, will be critical.

It is unfortunate that CDP could not be estimated for W1 due to the signal dropout problem. It would be interesting to see if its CDP were closer to W2, W3 and W4–7 or to W0 and WW. The former would be expected if the capping of the channels in W0 and WW is the cause of their higher CDP results. A method to repair the dropout data is being investigated.

It can be speculated that there is some transmission of cavitation acoustic emissions from the bulk volume through the channel to the exterior. If true it should apply to all WFTL targets and would infer a portion of the estimated CDP should be associated with cavitation activity in the channel. The size of that portion remains to be determined.

Analysis of all LDV data continues including application of wavelet techniques to better extract cavitation collapse emissions from the full bandwidth of velocity data.

CDP dependence on peak beam intensity, with total energy on target constant, indicates increased damage should be expected with greater intensity. Incubation phase damage, in terms of fraction of eroded area ( $A_e/A_0$ ), has been demonstrated to scale with damage potential by a power law dependence with exponent = 0.6 for type 316L stainless steel [3] (note Eq. (7) in [3] the right hand side should be  $C^* E^m$ ). Based on that scaling normalized fraction of area damage estimates for the intensity test targets are shown in Table 3. It is presumed here that the damage threshold value “ $E_{th}$ ” from [3] is very much smaller than CDP. Damage is predicted to be approximately 50% higher for RH compared to RM; RL damage should be about 15% less than RM.

Some measurable values of CDP were obtained from target RLDV for quite low pulse intensities, i.e. with charge as low as  $0.04 \mu\text{C}$  (1/100th a nominal WNR pulse). Similarly the passive cavitation transducers began to detect signals indicating cavitation at  $0.2 \mu\text{C}$ . At these low values the threshold for cavitation that can produce damage must be considered. The obtained CDP values at  $0.04 \mu\text{C}$  and even substantially larger charges are probably smaller than the threshold value  $E_{th}$ . Determination of the  $E_{th}$  value for this target was not part of the experiment scope and it would be a considerable effort to do so. Indeed,  $E_{th}$  depends on many specific target and irradiation conditions: geometry, vessel material and surface treatments, mercury flow, etc. The threshold for damage in the SNS target as a function of proton beam power remains an unknown quantity and one of the biggest uncertainty factors in estimating the target lifetime.

## 7. Conclusion

In-beam experiments investigating cavitation damage in short pulse mercury spallation targets were carried out at the WNR facility in LANSCE in 2008. A broad and complicated scope of objectives was carried out with emphasis on damage dependence on mercury flow velocity and on incident proton beam intensity. Analysis of damage on specimens from the test targets remains to be completed, but indirect measurements of cavitation activity were made and results are presented here for predicting relative damage between test conditions. Confirmation of the predictions from damage analysis is eagerly awaited.

## Acknowledgments

The authors extend their gratitude to supporting WNR experimenters Ashraf Abdou, Günter Bauer, Leonard Dial, Phil Ferguson, Van Graves, Shoichi Hasegawa, Hiroyuki Kogawa, Tom McManamy, Bob Sangrey and Dave West. The parallel beam diagnostic experiment was conducted by Tom Shea, Willem Blokland, Ralph Fiorito, Callie Goetz, Dinesh Pathak and Anatoly Shkvarunets. The support of LANSCE operations, safety and radiological staff was greatly appreciated as well as the technical assistance at the WNR from Leo Bitteker, Art Bridge, Gregg Chaparro and Steve Wender. The concept, development, data acquisition and analysis for passive cavitation detection in target RLDV is credited to Boston University collaborators Ron Roy, Robin Cleveland, Glynn Holt, Parag Chitnis, and Nick Manzi who was also an on-site WNR experimenter.

This work has benefited from the use of the Los Alamos Neutron Science Center at the Los Alamos National Laboratory. This facility is funded by the US Department of Energy.

## References

- [1] J.R. Haines, B.W. Riemer, D.K. Felde, J.D. Hunn, S.J. Pawel, Journal of Nuclear Materials 343 (2005) 58–69.
- [2] B.W. Riemer, J.R. Haines, J.D. Hunn, D.C. Lousteau, T.J. McManamy, C.C. Tsai, Journal of Nuclear Materials 318 (2003) 92–101.
- [3] M. Futakawa et al., Journal of Nuclear Materials 377 (2008) 182–188.

- [4] B. Riemer, J. Haines, M. Wendel, G. Bauer, M. Futakawa, S. Hasegawa, H. Kogawa, *Journal of Nuclear Materials* 377 (2008) 162–173.
- [5] T. McManamy, K.C. Goetz, T.J. Shea, in: *Eighth International Topical Meeting on Nuclear Applications and Utilization of Accelerators*, Pocatello, ID, 2007.
- [6] M.W. Wendel, D.K. Felde, T.P. Karnowski, B.W. Riemer, in: *2006 ASME Joint US European Fluids Engineering Summer Meeting*, July 17–20, 2006, Miami, Florida.
- [7] M. Wendel, D. Felde, B. Riemer, D. West, B. D'Urso, A. Ibrahim, in: *ASME Fluids Engineering Division Summer Conference*, August 10–14, 2008, Jacksonville, Florida.
- [8] A.A. Abdou, M. Wendel, D. Felde, B. Riemer, *ASME Fluids Engineering Division Summer Conference*, Vail, Colorado, USA, 2009.